

# Magnetized color superconducting cold quark matter within the $SU(2)_f$ NJL model: a novel regularization scheme

P. Allen<sup>a</sup>, A.G. Grunfeld<sup>a,b</sup> and N.N. Scoccola<sup>a,b,c</sup>

<sup>a</sup> *Department of Theoretical Physics,*

*Comisión Nacional de Energía Atómica,*

*Av.Libertador 8250, 1429 Buenos Aires, Argentina*

<sup>b</sup> *CONICET, Rivadavia 1917, 1033 Buenos Aires, Argentina*

<sup>c</sup> *Universidad Favaloro, Solís 453, 1078 Buenos Aires, Argentina*

## Abstract

The influence of intense magnetic fields on the behavior of color superconducting cold quark matter is investigated using an  $SU(2)_f$  NJL-type model for which a novel regulation scheme is introduced. In such a scheme the contributions which are explicitly dependent on the magnetic field turn out to be finite and, thus, do not require to be regularized. As a result of this, non-physical oscillations that might arise in the alternative regularization schemes previously used in the literature are naturally removed. In this way, a clearer interpretation of the physical oscillations is possible. The sensitivity of our results to the model parametrization is analyzed.

PACS numbers: 24.10.Jv, 25.75.Nq

## I. INTRODUCTION

At asymptotically large chemical potentials, the fact that cold quark matter behaves as a color superconductor can be shown by using perturbative methods in the context of quantum chromodynamics (QCD)[1]. However, such methods cannot be applied in the range of moderate densities relevant for, amongst others, the astrophysics of strongly magnetized compact stellar objects known as magnetars. We recall here that, although it is generally accepted that these objects can have surface magnetic fields up to  $10^{15}$  G[2], the estimates for the magnetic field values at their centers are model dependent to some extent, ranging between  $B \simeq 10^{18} - 10^{20}$  G (see e.g. Refs.[3–5]). Since the well-known sign problem prevents lattice QCD calculations from being performed at sufficiently low temperatures and finite chemical potential, one has to rely on effective models to analyze the behavior of magnetized quark matter in this region. One particular model that has been extensively used for this purpose is the Nambu-Jona-Lasinio (NJL) model[6]. This is an effective model originally devised to study the dynamics of chiral symmetry breaking, in which gluon degrees of freedom are integrated out and interactions are described by local four-quark interactions. The incorporation of additional diquark interactions into the model allows for the description of color superconducting matter[7]. In this context, the effect of a constant magnetic field has been analyzed by several authors [8–13]. At this point, it is important to remark that the local character of the interactions considered in the NJL-type models leads to divergences in the momentum integrals which need to be handled in some way in order to completely define the model and yield meaningful quantities. Several regularization procedures are possible even in the absence of magnetic fields [6]. Moreover, when magnetic field is introduced, the vacuum energy acquires a Landau level (LL) structure and an additional care is required in the treatment of the divergences. An elegant way of treating the regularization has been reported in Ref.[14] for the model in the absence of color superconductivity. The procedure follows the steps of the dimensional regularization prescription of QCD, performing a sum over all Landau levels in the vacuum term. This allows to isolate the divergence into a term that has the form of the zero magnetic field vacuum energy and that can be regularized in the standard fashion. It should be stressed that similar expressions for the magnetic field dependent terms can be obtained using a method based on the proper-time formulation[15]. So far, however, this procedure has not been applied to the case in which color superconduc-

tivity is present. Instead, existing calculations [9–13] remove the divergences by introducing some type of regulator function for each Landau level separately. This procedure, however, might in general introduce unphysical oscillations. A discussion on this can be found in Refs.[16–18], where it is also observed that the use of smooth regulator functions improve the situation. In fact, this allows to identify possible physical oscillations appearing in some cases[9, 10]. However, an even clearer interpretation of the results could be obtained if the unphysical oscillations were removed altogether with another scheme, especially at finite chemical potential and in the presence of color superconductivity. The main purpose of this work is to investigate the influence of a constant magnetic field on cold superconducting quark matter in the framework of the NJL-type model, using a regularization procedure in which the contributions that are explicitly dependent on the magnetic field turn out to be finite and, thus, do not required to be regularized. This procedure will be referred to as “Magnetic Field Independent Regularization” (MFIR), and it can be considered an extension of the method described in e.g. Ref.[14] to the case in which color pairing interactions are present. Since the aforementioned unphysical oscillations are completely removed in this scheme, we will complement our analysis by performing a detailed study of the resulting cold matter phase diagrams, including their dependence on the parameters of the model and, in particular, the coupling strength of the diquark interactions. Being mostly concerned with the issues related to the model regularization procedure we will, for simplicity, assume all the quark species to have a common chemical potential leaving the incorporation of the neutrality and  $\beta$  equilibrium conditions relevant for stellar matter applications for future studies.

We organize the article as follows. In Section II we present the Nambu Jona Lasinio model with magnetic field and diquark interactions. In particular, we briefly review the regularization schemes used in the literature and describe in some detail the MFIR scheme introduced in this work. The model parameters used in our numerical calculations are also given. In Sect. III we compare our results for the behavior of the cold and dense magnetized quark matter with those previously reported in the literature. In Sect. IV we present results for the phase diagrams in the  $\tilde{e}B - \mu$  plane as obtained using MFIR for different interaction coupling ratios and parameter sets. In Sect. V we present our conclusions. Finally, in the Appendix, several details of the formalism of the MFIR scheme are described.

## II. MAGNETIZED COLD QUARK MATTER WITHIN THE $SU(2)_f$ NJL MODEL IN THE PRESENCE OF COLOR PAIRING INTERACTIONS

### A. The thermodynamical potential in the mean field approximation

We consider a NJL-type  $SU(2)_f$  Lagrangian density which includes scalar-pseudoscalar and color pairing interactions. In the presence of an external magnetic field and chemical potential it reads:

$$\mathcal{L} = \bar{\psi} \left[ i \tilde{\mathcal{D}} - m_c + \mu \gamma^0 \right] \psi + G \left[ (\bar{\psi}\psi)^2 + (\bar{\psi}i\gamma_5\vec{\tau}\psi)^2 \right] + H \left[ (i\bar{\psi}^C \epsilon_f \epsilon_c^3 \gamma_5 \psi)(i\bar{\psi} \epsilon_f \epsilon_c^3 \gamma_5 \psi^C) \right]. \quad (1)$$

Here,  $G$  and  $H$  are coupling constants,  $\psi = (u, d)^T$  represents a quark field with two flavors,  $\psi^C = C\bar{\psi}^T$  and  $\bar{\psi}^C = \psi^T C$ , with  $C = i\gamma^2\gamma^0$ , are charge-conjugate spinors and  $\vec{\tau} = (\tau_1, \tau_2, \tau_3)$  are Pauli matrices. Moreover,  $(\epsilon_c^3)^{ab} = (\epsilon_c)^{3ab}$  and  $(\epsilon_f)^{ij}$  are antisymmetric matrices in color and flavor space respectively. Furthermore,  $m_c$  is the (current) quark mass that we take to be the same for both flavors and  $\mu$  is the quark chemical potential. The coupling of the quarks to the electromagnetic field  $\tilde{\mathcal{A}}_\mu$  is implemented through the covariant derivative  $\tilde{D}_\mu = \partial_\mu - i\tilde{e}\tilde{Q}\tilde{\mathcal{A}}_\mu$ . Note that here we are dealing with “rotated” fields. In fact, as is well known, in the presence of a non-vanishing superconducting gap  $\Delta$ , the photon acquires a finite mass. However, as shown in Ref.[19], there is a linear combination of the photon and the eighth component of the gluon field that leads to a massless rotated  $U(1)$  field. The associated rotated charge matrix  $\tilde{Q}$  is given by

$$\tilde{Q} = Q_f \otimes 1_c - 1_f \otimes \left( \frac{\lambda_8}{2\sqrt{3}} \right) \quad (2)$$

where  $Q_f = \text{diag}(2/3, -1/3)$  and  $\lambda^8$  is the color quark matrix  $\lambda_8 = \text{diag}(1, 1, -2)/\sqrt{3}$ . Then, in a six dimensional flavor-color representation  $(u_r, u_g, u_b, d_r, d_g, d_b)$ , the rotated  $\tilde{q}$  for different quarks are:  $u_r = 1/2, u_g = 1/2, u_b = 1, d_r = -1/2, d_g = -1/2, d_b = 0$ . The rotated unit charge  $\tilde{e}$  is given by  $\tilde{e} = e \cos \theta$ , where  $\theta$  is the mixing angle which is estimated to be  $\simeq 1/20$ [20]. In the present work we consider a static and constant magnetic field in the 3-direction,  $\tilde{\mathcal{A}}_\mu = \delta_{\mu 2} x_1 B$ , which in fact is also a mixture of the electromagnetic field and color fields.

In what follows we work in the mean field approximation (MFA), assuming that the only non-vanishing expectation values are  $\langle \bar{\psi}\psi \rangle = -(M - m_c)/2G$  and  $\langle i\bar{\psi}^C \epsilon_f \epsilon_c^3 \gamma_5 \psi \rangle =$

$-\Delta/2H$ , which can be chosen to be real. Here,  $M$  and  $\Delta$  are the so-called dressed quark mass and superconducting gap, respectively. The resulting MFA thermodynamic potential at vanishing temperature reads

$$\Omega_{\text{MFA}} = \frac{(M - m_c)^2}{4G} + \frac{\Delta^2}{4H} - \sum_{|\tilde{q}|=0, \frac{1}{2}, 1} P_{|\tilde{q}|} \quad (3)$$

where

$$P_{|\tilde{q}|=0} = \int \frac{d^3p}{(2\pi)^3} [E_0^+ + |E_0^-|], \quad (4)$$

$$P_{|\tilde{q}|=1} = \frac{\tilde{e}B}{8\pi^2} \sum_{k=0}^{\infty} \alpha_k \int_{-\infty}^{\infty} dp_z [E_1^+ + |E_1^-|], \quad (5)$$

$$P_{|\tilde{q}|=1/2} = \frac{\tilde{e}B}{4\pi^2} \sum_{k=0}^{\infty} \alpha_k \int_{-\infty}^{\infty} dp_z [E_{1/2}^+ + E_{1/2}^-]. \quad (6)$$

Here, we have introduced  $\alpha_k = 2 - \delta_{k0}$  and

$$\begin{aligned} E_0^\pm &= \sqrt{p^2 + M^2} \pm \mu \\ E_1^\pm &= \sqrt{p_z^2 + 2k\tilde{e}B + M^2} \pm \mu \\ E_{1/2}^\pm &= \sqrt{\left[ \sqrt{p_z^2 + k\tilde{e}B + M^2} \pm \mu \right]^2 + \Delta^2}. \end{aligned} \quad (7)$$

Clearly, Eqs.(4-6) are divergent and, thus, require to be regularized. Some alternative schemes to achieve this will be discussed in the following subsection. Given the corresponding regularized form  $\Omega_{\text{MFA}}^{\text{reg}}$ , the associated gap equations for  $M$  and  $\Delta$  then read

$$\frac{\partial \Omega_{\text{MFA}}^{\text{reg}}}{\partial(M, \Delta)} = 0. \quad (8)$$

For each value of  $\mu$  and  $\tilde{e}B$ , several solutions of these equations will generally exist, corresponding to different possible phases, and the most stable solution is that associated to the absolute minimum of the thermodynamic potential.

## B. Regularization schemes

As already mentioned, the contributions from Eqs.(4-6) need to be regularized. In previous studies[9–13] this was accomplished by introducing some cutoff function  $h_\Lambda(q)$  in the corresponding integrands, with  $q = p$  in the case of Eq.(4) and  $q = \omega_{p_z, k} \equiv \sqrt{p_z^2 + 2k|\tilde{q}|B}$  for Eqs.(5,6). The obvious and simplest choice would be to take  $h_\Lambda(q) = \Theta(\Lambda - q)$ . In

what follows, we will refer to this regularization scheme as “sharp function regularization” (ShFR). In this case, the integral in Eq.(4), which is magnetic field independent, is cut off when  $p = \Lambda$ . The contributions coming from Eqs.(5-6) include a sum over Landau levels, and the integral in each of these is cut off for the  $p_z$  that satisfies  $\Lambda = \sqrt{p_z^2 + 2k|\tilde{q}|B}$ , that is, such that the momentum and magnetic field contribution to the quark dispersion relation does not exceed the value of the cut-off. This would seem like a natural way of extending the 3D sharp cutoff zero magnetic field regularization to the finite  $\tilde{e}B$  case. However, the magnetic field dependence of the prescription brings in strong unphysical oscillations. To minimize the effects of this magnetic field dependence, the aforementioned studies have been carried out replacing the Heaviside function with a smooth regulator. For definiteness in this work, we consider the function  $h_\Lambda(q) = 1/(1 + \exp[(q/\Lambda - 1)/a])$ . We have verified that other possible choices lead to similar results. To choose the value of the constant  $a$  that determines the regulator smoothness one is limited by the fact that a too steep function does not improve over the ShFR results and that a too smooth function leads to values of the quark condensate in absence of the magnetic field which are quite above the phenomenological range. Here, we follow Refs.[11, 12] and consider  $a = 0.05$ . In what follows we will refer to this regularization scheme as “smooth function regularization” (SmFR). The similarities and differences in the results yielded by the two regularization schemes introduced so far will be discussed in the following section. There it will be noted that, although somewhat suppressed, the undesired oscillations are still present in SmFR. It is important to remark at this stage that  $P_{|\tilde{q}|=0,1}$  can be rewritten in terms of a vacuum and a matter contribution, of which only the first one is divergent. Thus, there is certain ambiguity on whether the regularization function has to be included in the matter term or not. Having analyzed both possibilities, we verified that in our case, this ambiguity amounts at most to small quantitative differences. The results to be presented correspond to the case where only the vacuum energy is regularized.

To fully get rid of the above mentioned regularization artifacts, we introduce in what follows an alternative scheme in which the contributions that are explicitly dependent on the magnetic field turn out to be finite and thus do not need to be regularized. We will refer to this regularization scheme as “magnetic field independent regularization” (MFIR). We start by considering the  $P_{|\tilde{q}|=0}$  contribution. Since it is independent of the magnetic field, it can be treated in the usual way [6]. Introducing a sharp 3D cutoff we get

$$\begin{aligned}
P_{|\tilde{q}|=0} &= \frac{1}{\pi^2} \int_0^\Lambda dp p^2 \sqrt{p^2 + M^2} \\
&+ \frac{\Theta(\mu - M)}{\pi^2} \left[ \frac{\mu(\mu^2 - M^2)^{3/2}}{3} - \frac{(\mu^2 - M^2)^2}{8} h \left( \frac{M}{\sqrt{\mu^2 - M^2}} \right) \right], \quad (9)
\end{aligned}$$

where  $h(z) = (2 + z^2)\sqrt{1 + z^2} + z^4 \ln[z/\sqrt{1 + z^2}]$ .

In the case of  $P_{|\tilde{q}|=1}$  we note that, except for the specific value of the quark charge, the corresponding expression coincides with that analyzed in Ref.[14] where no color pairing interactions were considered. Following the steps discussed in that reference we get

$$\begin{aligned}
P_{|\tilde{q}|=1} &= \frac{1}{\pi^2} \int_0^\Lambda dp p^2 \sqrt{p^2 + M^2} + \frac{\tilde{e}B}{4\pi^2} \sum_{k=0}^{k_{max}} \alpha_k \left[ \mu \sqrt{\mu^2 - s_k^2} - s_k^2 \ln \left( \frac{\mu + \sqrt{\mu^2 - s_k^2}}{s_k} \right) \right] \\
&+ \frac{(\tilde{e}B)^2}{2\pi^2} \left[ \xi'(-1, x) + \frac{x - x^2}{2} \ln x + \frac{x^2}{4} \right] \quad (10)
\end{aligned}$$

where  $x = M^2/(2\tilde{e}B)$ ,  $k_{max} = \text{Floor}[(\mu^2 - M^2)/(2\tilde{e}B)]$  and  $s_k = \sqrt{M^2 + 2k\tilde{e}B}$ . In Eqs.(9-10), the first term is a vacuum contribution which does not explicitly depend on the magnetic field and the second term is the matter contribution. The last term in Eq.(10) is the explicit magnetic field contribution to the vacuum, which has been isolated into a finite term.

The case of  $|\tilde{q}| = 1/2$  is more involved. However, as discussed in detail in the Appendix, it can be cast into the form

$$\begin{aligned}
P_{|\tilde{q}|=1/2} &= \frac{2}{\pi^2} \int_0^\Lambda dp p^2 (E_\Delta^+ + E_\Delta^-) + \frac{(\tilde{e}B)^2}{2\pi^2} \left[ \xi'(-1, y) + \frac{y - y^2}{2} \ln y + \frac{y^2}{4} \right] \\
&+ \frac{(\tilde{e}B)^2}{2\pi^2} \int_0^\infty dp \left[ \sum_{k=0}^\infty \alpha_k f(p^2 + k) - 2 \int_0^\infty dx f(p^2 + x) \right] \quad (11)
\end{aligned}$$

where  $E_\Delta^\pm = \sqrt{(\sqrt{p^2 + M^2} \pm \mu)^2 + \Delta^2}$ ,  $y = (M^2 + \Delta^2)/(\tilde{e}B)$  and

$$f(z) = \sum_{s=\pm 1} \left[ \sqrt{(\sqrt{z + 2x} + s \mu/\sqrt{\tilde{e}B})^2 + y - 2x - \sqrt{z + y}} \right]. \quad (12)$$

In this expression a 3D sharp cutoff has been introduced to regularize the first term, i.e. the one that contains contributions from the vacuum and matter which do not explicitly depend on the magnetic field. Note that, as in the case of vanishing  $\tilde{e}B$  discussed in e.g. Ref.[21], these cannot be disentangled into two terms unless  $\Delta = 0$ . The second term is the vacuum magnetic contribution analogous to the  $|\tilde{q}| = 1$  case. Finally, the third term is an additional explicitly magnetic field dependent matter contribution which, as shown in the Appendix, turns out to be finite.

### C. Model parametrization

In order to analyze the dependence of the results on the model parameters, we will consider two  $SU(2)_f$  NJL model parameterizations. Set 1 corresponds to that leading to  $M_0 = 340$  MeV while set 2 to that leading to  $M_0 = 400$  MeV, within the MFIR regularization. Here,  $M_0$  represents the vacuum quark effective mass in the absence of external magnetic fields. The corresponding model parameters are listed in Table I.

TABLE I. Parameter sets for the  $SU(2)_f$  NJL model. In both cases, empirical values in vacuum for the pion observables are reproduced,  $m_\pi = 138$  MeV and  $f_\pi = 92.4$  MeV.

Parameter set	$M_0$	$m_c$	$G\Lambda^2$	$\Lambda$	$-\langle u\bar{u} \rangle^{1/3}$
	MeV	MeV		MeV	MeV
Set 1	340	5.595	2.212	620.9	244.3
Set 2	400	5.833	2.440	587.9	240.9

We should observe that in the  $\tilde{e}B = 0$  limit, ShFR and MFIR regularization schemes result in the same mass. On the other hand, the masses for SmFR are about 10 MeV larger for both sets of parameters. This happens because the regulator function has a non-zero tail for large momentum with respect to the ShFR case, which causes the contribution from the vacuum to be larger, thus giving rise to a somewhat larger dressed mass.

## III. NUMERICAL RESULTS

### A. Comparison between regularization schemes

To motivate the introduction of the MFIR scheme, in this subsection we will compare the resulting predictions with the ones of the ShFR and SmFR. For definiteness, we will consider set 1 and take  $H/G = 0.75$ , value that follows from various effective models of quark-quark interactions[7]. In addition, some general features of the results will be described.

In Fig. 1, we plot the results for  $M$  and  $\Delta$  as a function of  $\mu$ , for all three regularizations. At a fixed magnetic field, these would appear to present similar behaviors. Two distinct types of phases exist in all cases: on the one hand, for low chemical potential, chiral symmetry is



broken and superconducting effects are absent. Since  $M > \mu$ , all matter terms are zero and the dressed mass is independent of the chemical potential. This phase, to be denoted as B phase as in previous studies[15, 22–25], always exists for a low enough chemical potential. If chemical potential is increased, on the other hand, there will be a first order phase transition (whose critical chemical potential  $\mu_c$  depends on the regularization) to a phase where  $\Delta$  is non vanishing and the dressed mass is small. It is considered to be a restored symmetry phase, even though exact symmetry restoration occurs only if  $m_c = 0$ . Since in our case the current quark mass is finite but small, restoration is only approximate. For higher chemical potentials, further transitions may appear within the  $\Delta \neq 0$  region, causing it to have a substructure consisting of several phases. One of such transitions can be seen in the upper left panel of Fig. 1, signalled by a small kink in the mass at  $\mu_c = 334.9$  MeV. To understand the origin of these we must recall that, for the quark species with  $|\tilde{q}| = 1/2$  and 1, the dispersion relations acquire a Landau level structure due to the magnetic field, as seen in Eq.(7). Let us consider first the case  $|\tilde{q}| = 1$ , where in the matter contribution to the thermodynamic potential a sum over these Landau levels up to  $k_{max}$  has to be performed. Here,  $k_{max}$  is determined by the chemical potential, mass and magnetic field. Namely,  $k_{max} = \text{Floor}[(\mu^2 - M^2)/(2\tilde{e}B)]$ . Following the notation of previous works, a chirally restored phase where the LL's are populated up to a given  $k$  will be referred to as an  $A_k$  phase, even though we bear in mind that this phase is qualitatively different in that there is a finite diquark gap now. The kink in Fig. 1 then corresponds to a transition in which the highest LL that is populated (given by  $k_{max}$ ) changes in one unit. In what follows, we will refer to these as “van Alphen-de Haas (vAdH) transitions”. It is also clarifying to mention that the dressed mass vanishes in the chiral case, so the vAdH transitions are actually signalled by discontinuities in the density, and that for the  $k^{th}$  LL they are simply given by the relation  $\mu = \sqrt{2k|\tilde{q}|B}$ . In the non-chiral case there will be a small departure from this relation originating from the finite mass in the restored phase. It is important to stress that out of the quark species with different values of  $|\tilde{q}|$ , the only one that produces vAdH transitions is  $|\tilde{q}| = 1$ . In fact,  $|\tilde{q}| = 0$  quarks are decoupled from the magnetic field, so their dispersion relation is the same as in the zero magnetic field case. Moreover, quarks with  $|\tilde{q}| = 1/2$  have an altogether different behavior. The coupling of this quark species to the  $\Delta$  removes the theta functions from the sum, much in the same way that a theta function becomes a Fermi-Dirac distribution when temperature is introduced. Hence, there is no cut off in the

sum over LLs, which means that when  $\Delta$  is finite there is non-zero density for all levels.

Now, even though the order parameters have similar behaviors at a fixed  $\tilde{e}B$  as a function of chemical potential, the three regularizations exhibit important qualitative differences along the magnetic field axis, as can be seen in Figs. 2 and 3. Regularization schemes ShFR and SmFR exhibit non-physical oscillations, whose origin lies in the magnetic field dependence of the regularization in the vacuum term, that causes the contribution of a given LL to be larger for lower magnetic fields. This can be most clearly appreciated in Fig. 2, which displays the behavior of  $M$  as a function of  $\tilde{e}B$  for  $\mu = 0$ . Here, the only contribution to the thermodynamic potential comes from the regularized vacuum. In the ShFR, which is the most extreme case, the only LLs participating in the sum are those for which  $\Lambda^2 \geq 2k|\tilde{q}|B$ . Hence, depending on the magnetic field, more or less terms appear and each time the relation is satisfied for a given  $k$ , there will be a discontinuity in the derivative of the thermodynamic potential. This singularity, hence, does not correspond to a phase transition. The soft regulator, which could be regarded as a way to handle this problem and remove sharp oscillations, still contains this pathology, because in this case the contribution of a given LL also depends on the magnetic field through the Fermi-type regulator function. So, even though the smooth integrals partly conceal this problem, the oscillations are still present and in Fig. 2 we can actually see that for ShFR and SmFR they are in phase. On the other hand, in the MFIR scheme the mass increases steadily with the magnetic field displaying the usual “magnetic catalysis effect” as in e.g. Refs.[14, 22, 24, 26].

The behavior of the vAdH transitions can also be appreciated in Fig. 3, where we plot  $M$  and  $\Delta$  as functions of  $\tilde{e}B$  for  $\mu = 400$  MeV. In the range  $\tilde{e}B = 0.01 - 0.1$  GeV<sup>2</sup> there is a set of peaked discontinuities, each of which corresponds to a vAdH transition. It should be emphasized that these are physical transitions, as opposed to the discontinuities previously discussed, since they correspond to values of  $\tilde{e}B$  at which the quark density for a given LL changes from zero to a finite number. Note that in the ShFR scheme they are harder to see because the non-physical oscillations originating from the vacuum contribution are of the same order of magnitude. In the MFIR scheme we can also observe that within each phase, for a given finite  $k$ , the mass tends to decrease when  $\tilde{e}B$  increases, but it shows a small increase before the next jump. In the  $k = 0$  phase, the mass decreases steadily with magnetic field as well. In the chirally restored phase, the superconducting gap will not vanish, and its behavior as a function of magnetic field is nontrivial, as shown in Fig. 3.

Also, note that  $\Delta$  is approximately constant in the range of  $\tilde{e}B \lesssim 0.12 \text{ GeV}^2$ , with small oscillations resulting from its coupling to the mass, and then presents a well-shaped curve.

The phase diagrams in the  $\tilde{e}B-\mu$  plane as obtained using the three different regularization schemes are displayed in Fig. 4. In the case of the ShFR and SmFR, we see that the oscillations in the order parameters induce oscillations in the critical chemical potential. These are small for low magnetic fields, but become larger in the intermediate  $\tilde{e}B$  range and once again make the phase diagram hard to interpret. As a result, we can also conclude that comparing the three regularizations for a given  $\tilde{e}B$ , as was done in Fig. 1, is actually misleading, since the oscillating behaviors in the order parameters and the critical chemical potential in ShFR and SmFR can cause the results to look quite different even for magnetic fields which are slightly different. In the MFIR scheme, we note that the critical chemical potential is approximately independent of  $\tilde{e}B$  for values below  $0.07 \text{ GeV}^2$ , then it decreases until it reaches a minimum near  $\tilde{e}B = 0.2 \text{ GeV}^2$  and after this value, it increases back again, giving rise to the usual well-shaped curve related to the “inverse magnetic catalysis effect” [27]. Due to the regulation artifacts, this feature is much less evident in the ShFR and SmFR. Concerning the vAdH transitions, which are the near vertical lines, we note that they are almost equal for the three prescriptions. In Fig. 4 they actually correspond to the MFIR case, but we make the observation that near the chiral restoration transition small deviations exist, which occur because the value of  $M$  that produces the deviation with respect to  $\sqrt{2k\tilde{e}B}$  is different in each scheme.

## B. MFIR results for different model parameters

In this subsection we further analyze the results obtained within the MFIR scheme, paying particular attention to their dependence on the model parameters. Results for the two parametrizations introduced in Sec.III.C will be given. Moreover, in the previous section only  $H/G = 0.75$  was considered. However, given that the value of this ratio is subject to certain degree of uncertainty, it is worthwhile to explore the consequences of varying it within a reasonable range. Thus, in what follows, the representative values  $H/G = 0.5, 0.75$  and 1 will be considered. A few comments on how the model results change for  $H/G < 0.5$  will be also made. Note that values  $H/G > 1$  are quite unlikely to be realized in QCD.

Let us start by analyzing the behavior of the order parameters as a function of  $\mu$  for

given values of magnetic field. We will concentrate on the results obtained with set 1, since it exhibits a more complex phase structure. Set 2 will be addressed further on. As was seen in the previous section for  $H/G = 0.75$ , the system is in the B phase for low  $\mu$ , where the dressed mass is large. On the other hand, it is in one of the possible A-type phases for a high enough  $\mu$  value where the dressed mass is small. However, if the coupling ratio is changed, other phases may appear for low  $\tilde{e}B$  values and intermediate chemical potentials. This can be seen in the left panels of Fig. 5, where  $\tilde{e}B = 0.04 \text{ GeV}^2$ . For  $H/G = 0.5$ , there is at  $\mu_c = 338.2 \text{ MeV}$  a weak first order transition from vacuum to a phase where the mass is slightly lower and also a slowly decreasing function of  $\mu$ . Quark density is finite for the  $|\tilde{q}| = 0$  and  $|\tilde{q}| = 1$  quarks (only the lowest LL being occupied for the latter species). Following Refs.[15, 22–25] this phase will be denoted as a C-type phase although, as in the case of the A-type phases, here the superconducting gap is non zero. Actually, it happens to be very small, remaining always under 1 MeV. Hence, it is not visible in this scale. If  $\mu$  is further increased, we find another first order transition to an A-type phase, at 346.1 MeV. However, we note that  $\Delta$  is in the range 25–30 MeV, which is a relatively small value compared to the resulting ones from higher coupling ratios in A-type phases. As the coupling constant ratio is increased from the value  $H/G = 0.5$ , the upper phase transition displaces downwards. This causes the C-type phase to shrink until it eventually disappears around  $H/G \sim 0.65$ , so that a single phase transition remains connecting the B phase to the A-type phases. As the coupling ratio is further increased, this phase transition continues to move downwards and for  $H/G = 0.75$ , the transition occurs at  $\mu_c = 333.6 \text{ MeV}$ . For even larger values of  $H/G$  ( $\sim 0.94$ ), the phase transition splits into two once again, so that for  $H/G = 1$  there is an intermediate phase, which will be referred to as a D phase. This phase is qualitatively different from the one found in  $H/G = 0.5$ . To begin with, the transition from vacuum to this phase is second order. The dressed mass is still large but the superconducting gap is finite and actually increases sharply with  $\mu$ . Since both condensates are appreciably large, this is usually referred to as a “mixed phase” [28], even though other meanings exist in the literature for this term [29]. There is no quark population for the  $|\tilde{q}| = 0$  and  $|\tilde{q}| = 1$  species, but the finiteness of  $\Delta$  induces a non-zero density for  $|\tilde{q}| = 1/2$  quarks. The transition leading to the A-type phases is first order as in the previous cases and  $\Delta \sim 175 \text{ MeV}$ . Within it, there is another transition for  $\mu = 308.5 \text{ MeV}$ , which is actually a vAdH being traversed vertically. The behavior is much simpler for  $\tilde{e}B = 0.3 \text{ GeV}^2$ , as can be seen in

the right panels of Fig. 5. For all values of the coupling ratio, we only see the B and  $A_0$  phases. Even though transitions to higher  $A_k$  phases will appear for much higher chemical potentials, it is generally seen that the phase structure is simpler for  $\tilde{e}B \gtrsim 0.15 \text{ GeV}^2$ , so that a single transition connecting the B phase to the  $A_0$  phase is seen in the range of  $\mu$  which is of interest (see [23] for a detailed discussion on how this occurs in NJL with magnetic field and without diquark pairing). For both magnetic fields, we see that increasing  $H/G$  always produces larger values for  $\Delta$  and reduces the  $\mu_c$  necessary to achieve the superconducting phase. We should also note that for smaller magnetic fields,  $\Delta$  grows faster as a function of  $\mu$  than for  $\tilde{e}B = 0.3 \text{ GeV}^2$ , where it seems to be almost constant. As a matter of fact, we also checked that for magnetic fields larger than a value around  $0.4 \text{ GeV}^2$ , the superconducting gap actually decreases (yet only slightly) with chemical potential.

A deeper understanding of the behavior of the phases can be obtained from the phase diagrams in the  $\tilde{e}B - \mu$  plane (Fig. 6), where our three coupling ratios and both parameter sets are considered. The first transition encountered if the phase diagram is traversed in the direction of increasing  $\mu$  will be referred to as the “main transition”. It has approximately the same shape in all displayed phase diagrams and it connects the B phase to populated phases in general. In set 2, the fact that  $M_0$  adjusts to a higher value causes the main transition to occur at a higher chemical potential. On the other hand, as  $H/G$  increases, the main transition is displaced downwards in its entirety, and the depth of the “inverse magnetic catalysis well” diminishes. In set 1, we can see for  $H/G = 0.5$  (top left panel) that both transitions enclosing the C-type phase are constant in a large magnetic field range so that it extends in an approximately horizontal band up to  $\tilde{e}B \simeq 0.11 \text{ GeV}^2$ , where it is bounded by a crossover type transition, signalled by the peak of the chiral susceptibility. The crossover leads to an  $A_0$  phase and, as expected, the mass drops sharply and  $\Delta$  increases. The different possible criteria to define this kind of transitions were discussed in detail in [23]. On the other hand, if magnetic field is decreased down to zero, the two horizontal transitions continue to exist (however, the lower transition becomes second order when  $\tilde{e}B = 0$ ), which means that a phase with large mass and quark population exists in the NJL model without magnetic field. The detailed behavior of the C-type region is rather involved in the limiting case in which  $\tilde{e}B$  tends to zero, and will not be discussed any further. It is important to point out that the existence of C-type phases is not a consequence of the diquark pairing channels either. As a matter of fact, up to  $H/G = 0.5$  superconducting effects are still small, and the

phase diagram remains basically unchanged. In fact, the two roughly horizontal transition lines are seen to remain almost unmodified if the coupling ratio is swept between these two parameters. We observe that even though this C-type region consists of a single phase where only the lowest LL is populated (hence it is a  $C_0$  phase), the results from [23, 24] suggest that it may become more complex if vector interactions are introduced, or for parameter sets leading to a lower  $M_0$  value. In that case, it could be possible that  $C_k$  phases with higher  $k$ 's appear between the two horizontal transitions. In the A-type phases, higher LL population is allowed because the mass is lower than in the C-type phases. vAdH transitions separate phases with different number of LL populated, and in the presented diagrams, LL's up to  $k = 7$  are occupied by  $|\tilde{q}| = 1$  quarks. On the other hand, the phase diagram is simpler in set 2 (top right panel), where it is seen that there is no intermediate phase for  $H/G = 0.5$ . In [23] we showed that changing the parameter set so that  $M_0$  increases always produces a simpler phase structure where there are only a main transition and vAdH transitions. As has been said, the upper transition found in set 1 moves downwards when  $H/G$  is increased, so the  $C_0$  phase shrinks and finally disappears, leaving a rather simple phase structure for  $H/G = 0.75$  (middle-left) panel. Note that for this value of the coupling ratio the phase diagrams for both sets are qualitatively similar. Finally, the phase diagrams for  $H/G = 1$  are shown in the bottom panels, where the D phase is seen to exist for both parameter sets. Once again, we observe that the existence of this phase is a consequence of the diquark pairing alone and hence it already exists for  $\tilde{e}B = 0$ . It is interesting to note, however, that it continues to exist for finite magnetic fields. The two transitions delimiting it are roughly horizontal for low  $\tilde{e}B$ . For higher values, the transitions lines move closer together and finally intersect near  $0.1 \text{ GeV}^2$  causing the D phase to disappear. At low magnetic field, the D phase exists for a narrow  $\mu$  range of at most 5 MeV for either set, but larger values of  $H/G$  would cause the phase to extend farther in the chemical potential direction.

In Fig. 7, we present the behavior of the order parameters as a function of magnetic field, for all considered values of  $H/G$  and representative values of  $\mu$ . Once again, we display the results for set 1 only, since no qualitatively different behaviors arise for set 2. It was already seen in Sec.III.A that in the B phase, mass increases with magnetic field and that  $\Delta = 0$ . This result, which is a manifestation of the magnetic catalysis effect, is exclusively seen in vacuum. Since  $\Delta = 0$  in this phase, the behavior is independent of  $H/G$ . When quark population is finite, several possibilities arise depending on the magnetic field,

parameter set and coupling constant. For high chemical potentials ( $\mu = 360$  MeV), where chiral symmetry is restored for all values of  $H/G$ , the mass exhibits a series of peak-like discontinuities. They correspond to the already discussed vAdH transitions, where the  $k_{max}$  corresponding to the  $|\tilde{q}| = 1$  quark changes in one unit. Due to the coupling to the mass,  $\Delta$  also oscillates. These oscillations become particularly large for intermediate magnetic field, around  $\tilde{e}B = 0.1$  GeV<sup>2</sup>. We note that on increasing  $H/G$ ,  $M$  is shifted downwards and  $\Delta$  is shifted upwards. Also, all oscillations are smoothed and become negligible compared to the scale of the order parameters.

For  $H/G = 0.5$ ,  $\mu = 340$  MeV corresponds to the intermediate C-type phase where quark population is finite and  $\Delta$  is small. We note that for  $\tilde{e}B$  near zero, the mass is close to the vacuum value, but gradually decreases as  $\tilde{e}B$  is increased. This feature is a manifestation of the anticatalysis effect. On the other hand,  $\Delta$  is very small and increases only slightly, always remaining under 1 MeV. The jumps in both  $M$  and  $\Delta$  near  $\tilde{e}B = 0.1$  GeV<sup>2</sup>, correspond to a first order transition to an A<sub>1</sub> phase. For larger magnetic fields, the mass decreases steadily until it finally returns to the B phase, which corresponds to the high magnetic field branch of the main transition. In the lower two panels of Fig. 7, we also see the behavior of  $M$  and  $\Delta$  in the mixed phase for  $H/G = 1$ . Here, we can see that the mass is almost independent of magnetic field in the D phase (slightly decreasing), while the superconducting gap increases from 25 MeV to 50 MeV. A few comments should be made regarding the vAdH transitions. These transitions are a characteristic of the chirally restored region of any NJL model with magnetic field. In particular, in the model without diquark pairing, there will be vAdH transitions for up quarks and down quarks. In the rotated base, quarks with charges  $|\tilde{q}| = 1$  and  $|\tilde{q}| = 1/2$  couple to the magnetic field, of which only the former yield first order transitions. However, there is a vAdH-like cross over transition for  $H/G = 0.5$  and  $0.75$  that resembles a  $|\tilde{q}| = 1/2$  vAdH in the following sense. If we were to set  $H = 0$ , then  $\Delta = 0$ , and the integrals in the  $|\tilde{q}| = 1/2$  matter terms would transform to Heaviside functions, cutting off the LL sum at a maximum  $k$  given by the relation  $\sqrt{\mu^2 - (M^2 + k\tilde{e}B)}$  and therefore producing vAdH transitions. If  $H/G$  is made finite but small, these discontinuities quickly disappear, but a remnant of these transitions is still present because the associated quark number susceptibility still exhibits peaks. However, they are smeared out as  $H/G$  is increased and for  $H/G = 0.5$  there is no trace left of these transitions, except for the one corresponding to the LL passage from 0 to 1. In set 1, we can see that this transition is

first order and has an end point after which it becomes a cross over, as can be seen in the corresponding panel in Fig. 6. This crossover is still present for  $H/G = 0.75$  and finally disappears for  $H/G = 1$ . We make the observation that since these are rather weak, we do not consider them to separate distinct phases.

#### IV. SUMMARY AND CONCLUSIONS

In the present work we explored the effects of magnetic field on cold color superconducting quark matter in the framework of the NJL-type model, using a regularization scheme in which the contributions which are explicitly dependent on the magnetic field turn out to be finite and, thus, do not require to be regularized. Such a “magnetic field independent regularization” (MFIR) scheme can be considered an extension of the method described in e.g. Ref.[14] to the case in which color pairing interactions are present. We compared the corresponding results with those obtained through the regularization methods used in previous works[9–13]. In those works, a regulator function was introduced in order to separately render the contribution of each Landau level finite. This, however, might lead to the appearance of non-physical oscillations even when rather soft regulator functions are used, while within the MFIR scheme these oscillations are completely removed and, thus, results are easier to interpret. Note that in the cases we investigated the smooth regulator case exhibits barely no difference with respect to the MFIR scheme for  $\tilde{e}B$  up to  $0.1 \text{ GeV}^2$ , and the above mentioned oscillations start to become relevant from this value on. In respect of this, it should be borne in mind that some estimates[5] indicate that the magnetic fields at the center of magnetars can be as large as  $\tilde{e}B \sim 0.6 \text{ GeV}^2$ . The remaining of this paper was devoted to investigate, for the MFIR regularization scheme, the model parameter dependence of the behavior of magnetized cold superconducting quark matter. We considered two parameter sets that adjust to acceptable values of the dressed masses, and that were already known to generate qualitatively different phase diagrams in the non-superconducting case [23]. Moreover, three representative values of the coupling constant ratio  $H/G$  were considered. We found that up to  $H/G = 0.5$  superconducting effects are still small, and the phase diagram remains basically unchanged. In particular, for set 1 there is an intermediate phase, in which quark population exists but chiral symmetry is still strongly broken. The diquark gap in this phase is finite but extremely small. It is connected to other phases by first order



transitions and a chiral crossover. As the coupling ratio is increased, the two transitions surrounding this phase move close to each other, causing it to disappear at  $H/G \sim 0.65$ . A relatively simple phase diagram hence exists for a narrow range around the standard value  $H/G = 0.75$ . If the coupling ratio is increased beyond 0.94, a mixed phase is present in both parameter sets, where both condensates are large. This phase already exists for zero magnetic field and we showed that according to this model it extends in the magnetic field direction for a relatively large range of  $\tilde{e}B$ , disappearing for  $\tilde{e}B \sim 0.1\text{GeV}^2$ . It is bounded from below by a second order transition. The nature of the vAdH transitions was also discussed. We explained that in the rotated base these exist only for the  $|\tilde{q}| = 1$  quark, and that even though the  $|\tilde{q}| = 1/2$  quark couples to the magnetic field, its coupling to the superconducting gap smears the vAdH transitions out, leaving only a crossover remnant for the transition between the two lowest  $k$  values. Finally, we found that the inverse catalysis phenomenon is observed in all the cases, although less pronounced as  $H/G$  increases.

Throughout this work we have concentrated on the analysis of the impact of the novel regularization scheme on the model predictions for the effects of magnetic field on symmetric two flavor cold color superconducting quark matter. It is clear that, for applications in the physics of compact stars, the neutrality and  $\beta$ -equilibrium conditions should be taken into account. Moreover, to address the effect on the description of the CFL-type phases strangeness degrees of freedom have to be included. We expect to report on these topics in forthcoming publications.

## APPENDIX

In this Appendix we present some details concerning the derivation of Eq.(11). We start by considering Eq.(7). As a first step towards the regularization of this expression we sum and subtract the contribution for vanishing chemical potential. In this way we get

$$P_{|\tilde{q}|=1/2} = S_1 + S_2 \quad (13)$$

where

$$S_1 = \frac{\tilde{e}B}{\pi} \sum_{k=0}^{\infty} \alpha_k \int_{-\infty}^{\infty} \frac{dp_z}{2\pi} \sqrt{p_z^2 + k\tilde{e}B + M^2 + \Delta^2}. \quad (14)$$

and

$$S_2 = \frac{\tilde{e}B}{2\pi} \sum_{k=0}^{\infty} \alpha_k \int_{-\infty}^{\infty} \frac{dp_z}{2\pi} F(p_z^2 + k\tilde{e}B) \quad (15)$$

where

$$F(z) = \sum_{s=\pm 1} \left[ \sqrt{(\sqrt{z + M^2} + s \mu)^2 + \Delta^2} - \sqrt{z + M^2 + \Delta^2} \right]. \quad (16)$$

It is clear that both  $S_1$  and  $S_2$  are divergent. However  $S_1$  has the standard form analyzed in Ref.[14], with  $M^2 \rightarrow \Delta^2 + M^2$ . Thus, following the steps described in that reference we get

$$S_1 = \frac{4}{\pi^2} \int_0^\Lambda dp p^2 \sqrt{p^2 + M^2 + \Delta^2} + \frac{(\tilde{e}B)^2}{2\pi^2} \left[ \xi'(-1, y) + \frac{y - y^2}{2} \ln y + \frac{y^2}{4} \right] \quad (17)$$

where  $y = (M^2 + \Delta^2)/\tilde{e}B$  and, as in Ref.[14], a 3D sharp cutoff has been introduced to regularize the  $\tilde{e}B$ -independent contribution.

To regularize  $S_2$  we add and subtract the corresponding contribution in the absence of magnetic field. Namely,

$$S_2 = 4 \int \frac{d^3p}{(2\pi)^3} F(p^2) + R \quad (18)$$

where

$$R = \frac{\tilde{e}B}{2\pi} \sum_{k=0}^{\infty} \alpha_k \int_{-\infty}^{\infty} \frac{dp_z}{2\pi} F(p_z^2 + k\tilde{e}B) - 4 \int \frac{d^3p}{(2\pi)^3} F(p^2) \quad (19)$$

We prove in what follows that  $R$  is finite. For this purpose we start by rewriting its second term introducing cylindrical coordinates. Then, once the angular integral is performed we get

$$\int \frac{d^3p}{(2\pi)^3} F(p^2) = \int_{-\infty}^{\infty} \frac{dp_z}{2\pi} \int_0^{\infty} \frac{d\rho}{2\pi} \rho F(p_z^2 + \rho^2) = \frac{\tilde{e}B}{4\pi} \int_{-\infty}^{\infty} \frac{dp_z}{2\pi} \int_0^{\infty} dx F(p_z^2 + \tilde{e}Bx) \quad (20)$$

where the change of variables  $\rho = \sqrt{\tilde{e}Bx}$  has been used in the last step. Replacing this expression in Eq.(19) we get

$$R = \frac{\tilde{e}B}{2\pi} \int_{-\infty}^{\infty} \frac{dp_z}{2\pi} F(p_z^2) + \frac{\tilde{e}B}{\pi} \int_{-\infty}^{\infty} \frac{dp_z}{2\pi} \left[ \sum_{k=1}^{\infty} F(p_z^2 + k\tilde{e}B) - \int_0^{\infty} dx F(p_z^2 + \tilde{e}Bx) \right] \quad (21)$$

For convenience we introduce at this stage  $f(z) = F(\tilde{e}Bz)/\sqrt{\tilde{e}B}$  and perform the change of variables  $p = p_z/\sqrt{\tilde{e}B}$ . Then we get

$$R = \frac{(\tilde{e}B)^2}{2\pi^2} \int_0^{\infty} dp f(p^2) + \frac{(\tilde{e}B)^2}{\pi^2} \int_0^{\infty} dp \left[ \sum_{k=1}^{\infty} f(p^2 + k) - \int_0^{\infty} dx f(p^2 + x) \right] \quad (22)$$

where the fact that the integrands are even functions of  $p$  has been used. To proceed we notice that  $f(z)$  is bounded in the interval  $0 \leq z \leq \infty$ . Thus, to prove that the momentum integrals are convergent it is enough to verify that the corresponding integrands vanish

sufficiently fast as  $p \rightarrow \infty$ . For this purpose it is convenient to consider the expansion of  $f(z)$  for  $z \gg \mu^2/\tilde{e}B; (M^2 + \Delta^2)/\tilde{e}B$ . We get

$$f(z) = \sum_{m=1}^{\infty} \frac{C_m}{z^{m+1/2}} \quad (23)$$

where the values of  $C_m$  for  $m = 1, 2$  are

$$C_1 = \frac{\Delta^2 \mu^2}{(\tilde{e}B)^2} \quad ; \quad C_2 = \frac{\Delta^2 \mu^2}{(\tilde{e}B)^2} \left[ \frac{\mu^2}{\tilde{e}B} - \frac{3M^2 + \Delta^2}{2\tilde{e}B} \right] \quad (24)$$

It is clear from Eq.(23) that for large  $p$  the integrand in the first term of  $R$  goes as  $1/p^3$  and, thus, the corresponding integral is convergent. To prove the convergence of the second term one can proceed as follows. Let us consider  $N \gg \mu^2/\tilde{e}B; (M^2 + \Delta^2)/\tilde{e}B$  such that for  $z > N$  we can replace  $f(z)$  by the expansion Eq.(23). As an example, we note that for the range of values of  $\mu$  and  $\tilde{e}B$  considered in this work,  $\mu^2/\tilde{e}B$  and  $(M^2 + \Delta^2)/\tilde{e}B$  are always smaller than 25. Accordingly, we have checked that if  $N \gg 25$  (e.g.  $N=250$ ) the use of the first few terms in the expansion Eq.(23) leads to values which are in excellent agreement with those obtained from the full expression. Then, denoting by  $I$  the integrand in the second term of Eq.(22), we have

$$I = \left[ \sum_{k=1}^N f(p^2 + k) - \int_0^N dx f(p^2 + x) \right] + \sum_{m=1}^{\infty} C_m \left[ \sum_{k=N+1}^{\infty} \frac{1}{(p^2 + k)^{m+1/2}} - \int_N^{\infty} \frac{dx}{(p^2 + x)^{m+1/2}} \right] \quad (25)$$

Next we note that, since  $m \geq 1$ , the sum over  $k$  in the second term can be written in terms of the Hurwitz zeta function  $\xi$  and that the integral over  $x$  is convergent and can be explicitly performed. Consequently we get

$$I = \left[ \sum_{k=1}^N f(p^2 + k) - \int_0^N dx f(p^2 + x) \right] + \sum_{m=1}^{\infty} C_m \left[ \xi(m + 1/2, 1 + p^2 + N) - \frac{1}{m - 1/2} \frac{1}{(p^2 + N)^{m-1/2}} \right] \quad (26)$$

Considering values of  $p^2 \gg N$  and making again use of Eq.(23) it is easy to see that the two terms in the first bracket of Eq.(26) go as  $N/p^3$  which implies that their contributions to  $R$  are finite. What remains is to show that the leading contribution to the second bracket also goes faster than  $1/p$ . This is not so obvious since for  $m = 1$  the second term does go

as  $1/p$ . Actually, as shown in what follows we need this term to go like that in order to cancel a similar term arising from the first term. In fact this is the main reason why the subtraction scheme proposed in this work was introduced. To show how this cancellation occurs we consider the expansion of the Hurwitz zeta function. For  $x \gg 1$  and  $m \geq 1$  one has

$$\xi(m + 1/2, 1 + x) = \frac{x^{-(m-1/2)}}{m - 1/2} - \frac{x^{-(m+1/2)}}{2} + \mathcal{O}(x^{-(m+3/2)}) \quad (27)$$

Using this expansion it is easy to see that for  $p^2 \gg N$  we have

$$\xi(m + 1/2, 1 + p^2 + N) - \frac{1}{m - 1/2} \frac{1}{(p^2 + N)^{m-1/2}} \rightarrow -\frac{1}{2p^{2m+1}} + \mathcal{O}(p^{-(2m+3)}) \quad (28)$$

This implies that the leading contribution comes from the  $m = 1$  term and it goes as  $1/p^3$  ensuring the convergence of the corresponding integral.

Having proved that  $R$  is indeed finite only the first term in  $S_2$  requires regularization. Using a 3D sharp cutoff as before we get

$$S_2 = \frac{2}{\pi^2} \int_0^\Lambda dp p^2 \left[ E_\Delta^+ + E_\Delta^- - 2\sqrt{z + M^2 + \Delta^2} \right] + \frac{(\tilde{\epsilon}B)^2}{2\pi^2} \int_0^\infty dp \left[ \sum_{k=1}^\infty \alpha_k f(p^2 + k) - 2 \int_0^\infty dx f(p^2 + x) \right] \quad (29)$$

where, as defined in the main text,  $E_\Delta^\pm = \sqrt{(\sqrt{p^2 + M^2} \pm \mu)^2 + \Delta^2}$ . Finally, replacing Eqs.(17,29) in Eq.(13) we immediately get Eq.(11).

- 
- [1] D. Bailin and A. Love, Phys. Rept. **107**, 325 (1984).
  - [2] R. C. Duncan and C. Thompson, Astrophys. J. **392**, L9 (1992);
  - [3] D. Lai and S. L. Shapiro, Astrophys. J. **383**, 745 (1991);
  - [4] D. Bandyopadhyay, S. Chakrabarty and S. Pal, Phys. Rev. Lett. **79**, 2176 (1997) [astro-ph/9703066].
  - [5] E. J. Ferrer, V. de la Incera, J. P. Keith, I. Portillo and P. L. Springsteen, Phys. Rev. C **82**, 065802 (2010) [arXiv:1009.3521 [hep-ph]].
  - [6] U. Vogl and W. Weise, Prog. Part. Nucl. Phys. **27**, 195 (1991); S. Klevansky, Rev. Mod. Phys. **64**, 649 (1992); T. Hatsuda and T. Kunihiro, Phys. Rep. **247**, 221 (1994).
  - [7] M. Buballa, Phys. Rept. **407**, 205 (2005) [hep-ph/0402234].

- [8] E. J. Ferrer, V. de la Incera and C. Manuel, Phys. Rev. Lett. **95**, 152002 (2005) [hep-ph/0503162]; E. J. Ferrer and V. de la Incera, Lect. Notes Phys. **871**, 399 (2013) [arXiv:1208.5179 [nucl-th]].
- [9] J. L. Noronha and I. A. Shovkovy, Phys. Rev. D **76**, 105030 (2007) [Phys. Rev. D **86**, 049901 (2012)] [arXiv:0708.0307 [hep-ph]].
- [10] K. Fukushima and H. J. Warringa, Phys. Rev. Lett. **100**, 032007 (2008) [arXiv:0707.3785 [hep-ph]].
- [11] S. Fayazbakhsh and N. Sadooghi, Phys. Rev. D **82**, 045010 (2010) [arXiv:1005.5022 [hep-ph]].
- [12] S. Fayazbakhsh and N. Sadooghi, Phys. Rev. D **83**, 025026 (2011) [arXiv:1009.6125 [hep-ph]].
- [13] T. Mandal and P. Jaikumar, Phys. Rev. C **87**, 045208 (2013) [arXiv:1209.2432 [nucl-th]].
- [14] D. P. Menezes, M. Benghi Pinto, S. S. Avancini, A. Perez Martinez and C. Providencia, Phys. Rev. C **79**, 035807 (2009) [arXiv:0811.3361 [nucl-th]].
- [15] D. Ebert, K. G. Klimenko, M. A. Vdovichenko and A. S. Vshivtsev, Phys. Rev. D **61**, 025005 (2000) [hep-ph/9905253];
- [16] L. Campanelli and M. Ruggieri, Phys. Rev. D **80**, 034014 (2009) [arXiv:0905.0853 [hep-ph]].
- [17] M. Frasca and M. Ruggieri, Phys. Rev. D **83**, 094024 (2011) [arXiv:1103.1194 [hep-ph]].
- [18] R. Gatto and M. Ruggieri, Lect. Notes Phys. **871**, 87 (2013) [arXiv:1207.3190 [hep-ph]].
- [19] M. G. Alford, J. Berges and K. Rajagopal, Nucl. Phys. B **571**, 269 (2000) [hep-ph/9910254].
- [20] E. V. Gorbar, Phys. Rev. D **62**, 014007 (2000) [hep-ph/0001211].
- [21] D. Blaschke, M. K. Volkov and V. L. Yudichev, Eur. Phys. J. A **17**, 103 (2003) [hep-ph/0301065].
- [22] D. Ebert and K. G. Klimenko, Nucl. Phys. A **728**, 203 (2003) [hep-ph/0305149].
- [23] P. G. Allen and N. N. Scoccola, Phys. Rev. D **88**, 094005 (2013) [arXiv:1309.2258 [hep-ph]].
- [24] P. G. Allen, V. P. Pagura and N. N. Scoccola, Phys. Rev. D **91**, no. 11, 114024 (2015) [arXiv:1502.00572 [hep-ph]].
- [25] A. G. Grunfeld, D. P. Menezes, M. B. Pinto and N. N. Scoccola, Phys. Rev. D **90**, no. 4, 044024 (2014) [arXiv:1402.4731 [hep-ph]].
- [26] J. K. Boomsma and D. Boer, Phys. Rev. D **81**, 074005 (2010) [arXiv:0911.2164 [hep-ph]].
- [27] F. Preis, A. Rebhan and A. Schmitt, JHEP **1103**, 033 (2011) [arXiv:1012.4785 [hep-th]].
- [28] M. Huang, P. f. Zhuang and W. q. Chao, Phys. Rev. D **65**, 076012 (2002) [hep-ph/0112124].
- [29] F. Neumann, M. Buballa and M. Oertel, Nucl. Phys. A **714**, 481 (2003) [hep-ph/0210078].

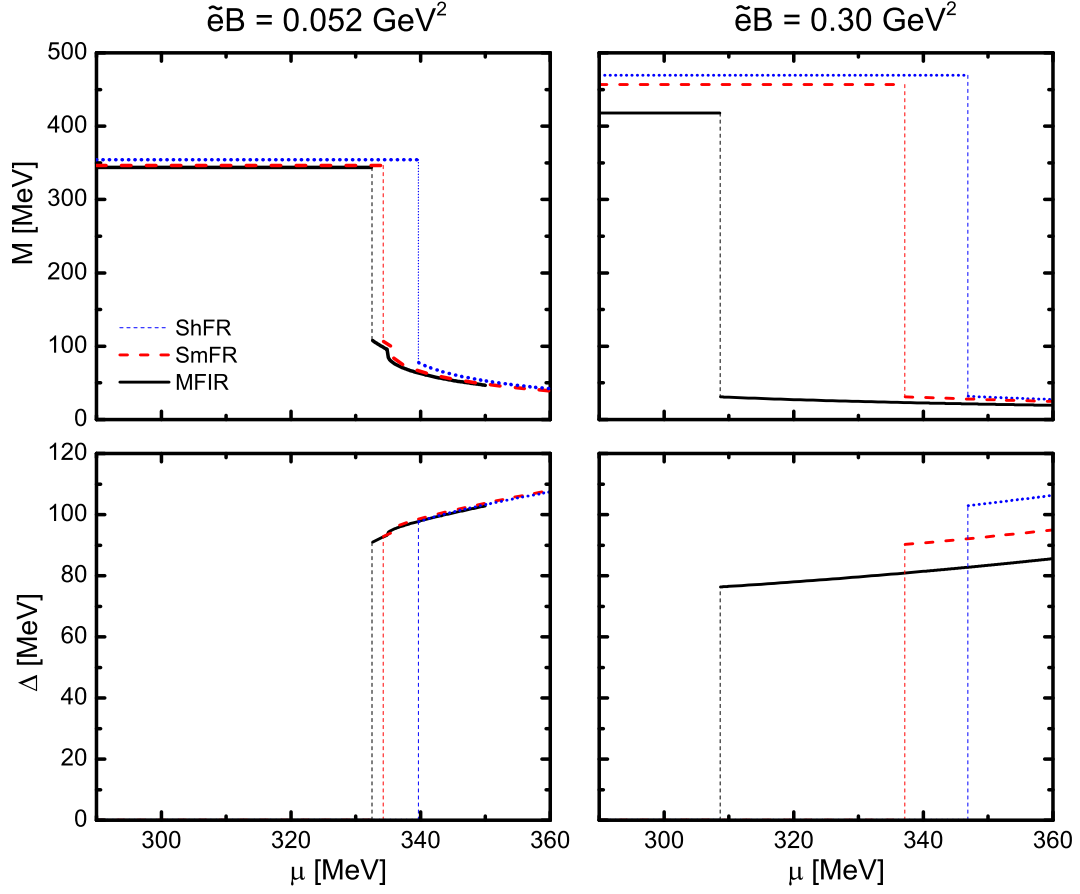


FIG. 1. Left panels:  $M$  vs  $\mu$  (upper) and  $\Delta$  vs  $\mu$  (bottom), for  $\tilde{e}B = 0.052 \text{ GeV}^2$ . Right panels:  $M$  vs  $\mu$  (upper) and  $\Delta$  vs  $\mu$  (bottom), for  $\tilde{e}B = 0.30 \text{ GeV}^2$ . Set 1 was used,  $H/G = 0.75$  and all regularization schemes considered.

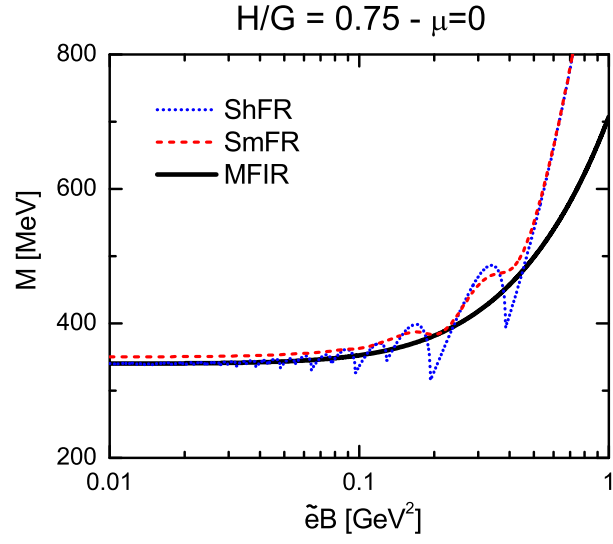


FIG. 2.  $M$  vs  $\tilde{e}B$  in the B phase, for the three regularization schemes considered, set 1 and  $H/G = 0.75$ . Note that  $\Delta = 0$  in this phase.

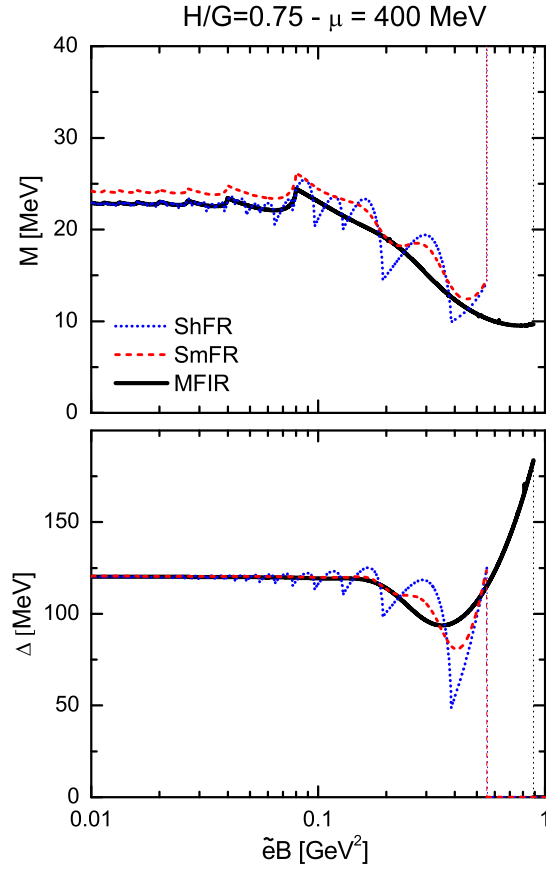


FIG. 3.  $M$  and  $\Delta$  vs  $\tilde{e}B$  in the A-type region, for the three regularization schemes considered, set 1 and  $H/G = 0.75$ .



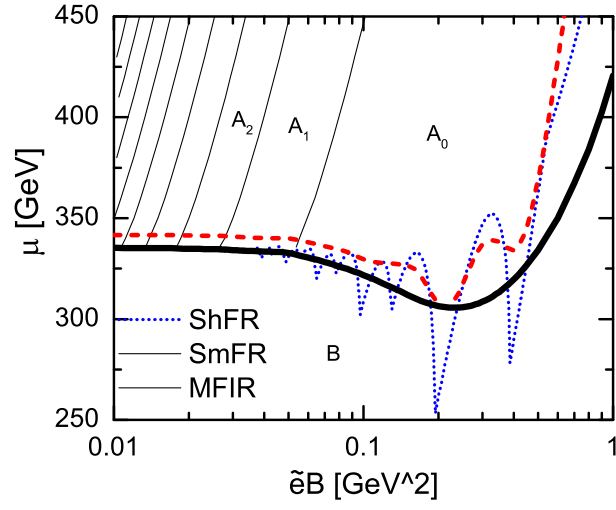


FIG. 4. Phase diagram in the  $\tilde{e}B$  vs  $\mu$  plane, for the three regularization schemes considered, set 1 and  $H/G = 0.75$ . All transitions seen in this diagram are first order.

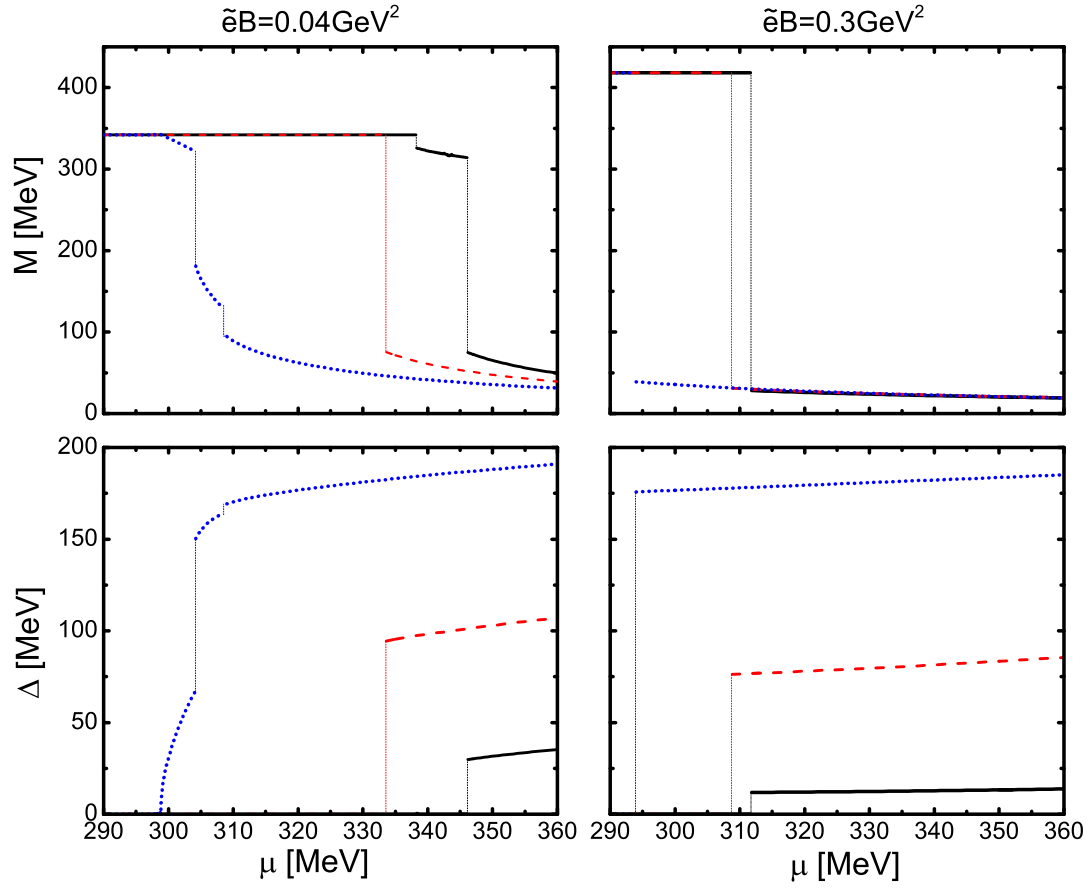


FIG. 5.  $M$  and  $\Delta$  vs  $\mu$  within the MFIR scheme for set 1, different  $H/G$  ratios and two values of  $\tilde{e}B$ . Full, dashed and dotted lines correspond to  $H/G = 0.5, 0.75$  and  $1$  respectively.

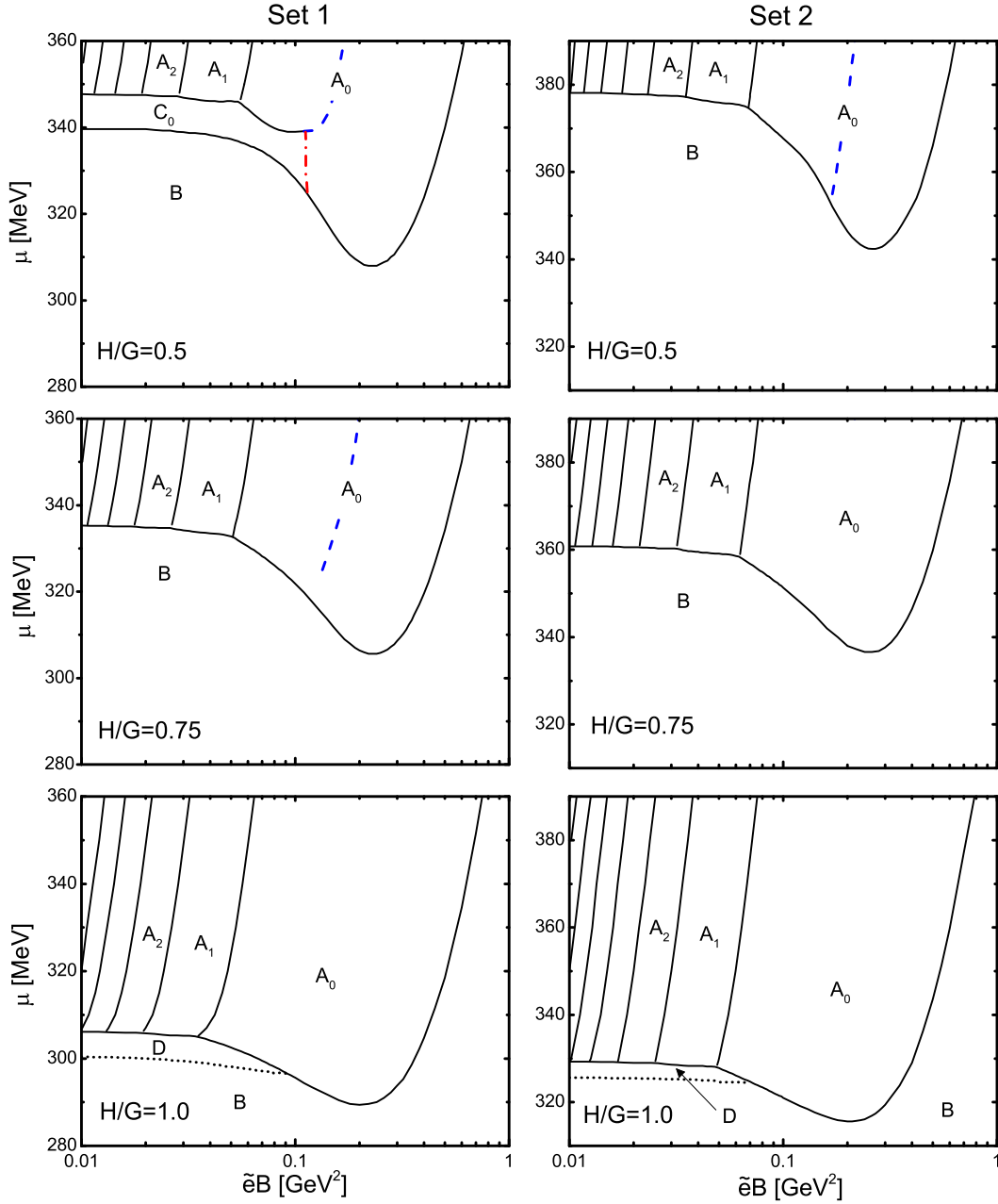


FIG. 6. Phase diagrams within the MFIR scheme for different  $H/G$  ratios, for both set 1 (left panels) and set 2 (right panels). Full black lines correspond to first order transitions and dotted black lines to second order transitions. The dash-dotted red lines represent chiral susceptibility crossovers. Blue dashed lines represent quark number susceptibility crossovers which are too weak to be actually considered to separate distinct phases. Note that the sets are plotted in different intervals of the  $\mu$  axis, even though the scale is the same.

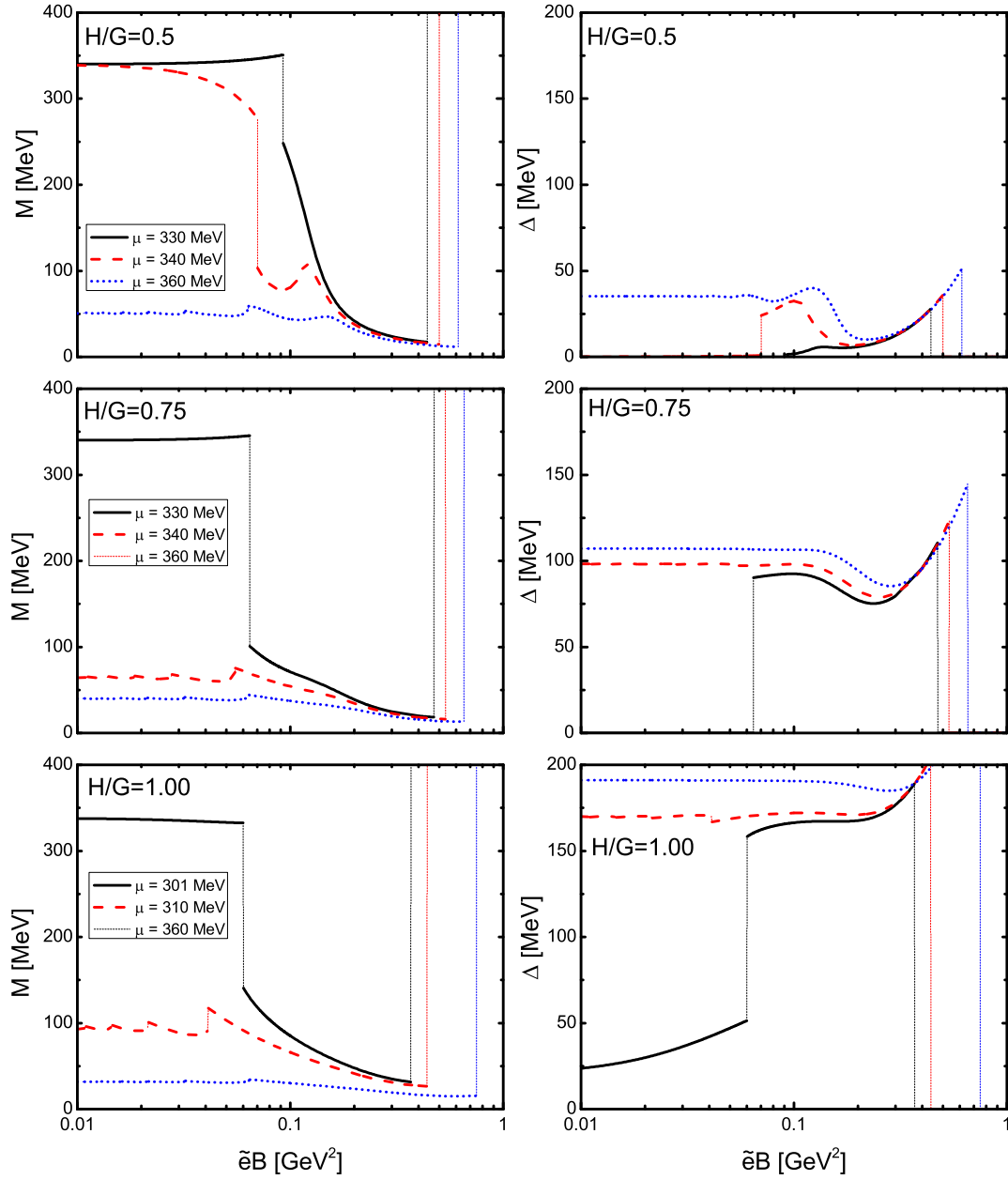


FIG. 7.  $M$  and  $\Delta$  vs  $\tilde{e}B$  within the MFIR scheme for the three values of  $H/G$  considered and several representative values of  $\mu$ , set 1.